Role of pore pressure on cracking and mechanical performance of concrete subjected to drying

François Soleilhet, Farid Benboudjema, Xavier Jourdain, Fabrice Gatuingt

Investigation of drying effects on cracking and mechanical performance of concrete

François Soleilhet[1], Farid Benboudjema[1], Xavier Jourdain[1], Fabrice Gatuingt[1]
[1] *LMT ENS-Paris-Saclay, France*

Abstract

Cement based material structures have to be managed over long periods. However, they are exposed to numerous loadings and present time-dependent deformations. In addition, the material is a porous medium in which pore pressure has an impact on macroscopic behaviour. The goal of this study is to better forecast the long term behaviour of cement based materials taking into account interactions between loads, time-dependent deformations and pore pressure. To do so, a previous model developed by the authors is extended to implement the impact of pore pressure on mechanical behaviour. Two applications are ran on a mature ordinary concrete. The damage state is clearly dependent of the mechanisms involved in the modelling. Considering pore pressure allows to find damage depth more accurate regarding experimental evidences. After a calibration of one test (at h_r= 45 %), we were able to predict the behaviour of other tests, with an underestimation of 10% on one sample where h_r changed. Interestingly, it was not manageable to use the same Biot parameter for the drying shrinkage and the mechanical modelling. As a result, by changing drastically the mechanical behaviour, the modelling of pore pressure is important to accurately assess the cracking state.

Keywords: Concrete, Cementitious Material, Drying Transport, Capillary Pressure, Eigen Stresses

1. Introduction

The long term management of key concrete structures (dams, power plant, nuclear waste facility disposal, large bridges) needs modelling to accurately predict cracking. This phenomenon is known to reduce drastically the lifespan of such struc-

tures. Today, mechanical loadings are rather well controlled with standards (Eurocode, ACI, JCI), whereas environmental actions (temperature, humidity) remain problematic. Strains related to temperature and humidity, both due to seasonal variations or human activities (cooling tower in the process of electricity generation), often present inadequate predictions of behaviour in service regarding cracking, in particular, structures with geometric differences that favour restrictions [1]. To account for all these loads, models have to be multi-physics.

An important feature of concrete material is the time-dependent strain which is a well known phenomenon that control the long term behaviour of the material [2, 3]. This includes creep, shrinkage and swelling. Moreover, cement based materials are porous medium. Initially saturated, they are the seat of water movements and exchanges with the ambient atmosphere. These exchanges generate eigen-stresses or cracking resulting from different mechanisms [4, 5]. This is a multi-scale problem. At the macroscopic scale, the impact of drying gradients related to shrinkage within the material will generate tensile stresses on the surface, which are self-equilibrated by compression of the core. In addition, strains incompatibilities occur between components: reinforcements and concrete [6], aggregates and cement pastes [7, 8, 9, 10] and incompatibilities due to different geometry and stiffness between concrete members [11, 12]. Finally, at nano-scale, drying modifies the physical characteristics of Calcium Silicate Hydrate (C-S-H) [13]. All of these have an impact on the serviceability, the mechanical performance of both the current loadings [14, 15, 16, 17] and the accidental loadings [18]. For some structures as dams, nuclear containment vessels, it may significantly increase concrete permeability and reduce tightness [19, 20]. It could also favour the penetration of aggressive species (carbonation, sulphate and chloride ions). Thus, to forecast the long term behaviour it is necessary to model hydric loading explicitly.

At a macroscopic level, there are many approaches in the literature which incorporate hydric loading. Uncoupled approaches are developed in structural design codes [21, 22] supposing homogeneous delayed strains. More complex approaches are requisite to account for heterogeneous strains. In a continuum framework [2, 23, 24, 25] or in discrete models [26, 27] many models have been developed

assuming that the total strain is split between the different delayed strains with no regard for capillary pressure. Others use poro-mechanics to distinguish the role of water (capillary, disjoining pressures) and the matrix [28, 29].

In this study, we extend a model previously developed at a macroscopic scale and in a continuum framework [23, 30, 31] to add to autogeneous, thermic, drying shrinkage and creep strains, the effects of hydric forces in the mechanical model. The first part of the paper is devoted to the description of the model constituve equations, with a special focus given on the incorporation of pore pressure's effects. A second part deals with numerical modelling. Those are performed under CAST3M software [32] and compared to a set of experimental data obtained on a mature ordinary concrete [17].

2. Hygro-mechanical modelling

2.1. General framework of modelling

The proposed model is based on the classical assumption of small strain. Under this hypothesis, total strain is decomposed in an elastic strain (ϵ_{el}) and in a various term of additional strains (Eq. 1).

$$\epsilon_t = \epsilon_{el} + \sum_i^n \epsilon_i \tag{1}$$

For the purpose of this work, drying shrinkage, creep and cracking are considered as additional strains. Hydration is not investigated and material properties are assumed at their final stage. Autogeneous shrinkage and thermal strains are not considered. These are motivated by the lack of information regarding hydration process on the isothermal experimental basis used for the model calibration. However, it is easy to add strains in this model as shown by Briffaut et al. [30]. Moreover, based on experimental evidences [33, 34], it is assumed that transport and mechanical phenomena are decoupled. As a result, the hygro-mechanical model developed in this paper is computed as a staggered problem weakly coupled as proposed in earlier studies [31, 35, 36].

2.2. Drying modelling

There are different approaches to model drying processes in the literature. These include models based on a diffusion equation written in either water content [37, 38, 39] or relative humidity [40]. There are more complex approaches based on modelling the transfer of different components within the porous material [41, 42, 43]. In this approach, the capillary pressure gradient is used as the main driving potential and the liquid and vapor water phases are modelled. It has shown to be adapted for high performances and ordinary concretes [41, 42, 43]. Thus, with the assumption of isothermal exchanges, in a mature material with a gas phase composed of a mixture of two perfect gases (dry air and water vapour) and neglecting the Darcean transport of the gas in front of the diffusion of water vapour, the drying state is governed by the differential equation (2).

$$\phi\left(1-\frac{\rho_v}{\rho_w}\right)\frac{\partial S_w}{\partial P_c}\frac{\partial P_c}{\partial t}=\mathrm{div}\left[\left(\frac{k_{rl}(S_w)K_w^{int}}{\mu_w}+\frac{d_{rl}(S_w)D_v^{int}P_{vs}}{\rho_w^2}\left(\frac{M_v}{RT}\right)^2\exp^{-\frac{P_c}{\rho_w}\frac{M_v}{RT}}\right)\nabla\mathbf{P_c}\right] \tag{2}$$

where ρ_w ($\mathrm{kg\,m^{-3}}$), ρ_v ($\mathrm{kg\,m^{-3}}$), μ_w ($\mathrm{Pa\,s}$), ϕ(-), M_v ($\mathrm{g\,mol^{-1}}$), R ($\mathrm{J\,K^{-1}\,mol^{-1}}$), T (K), P_{vs} (Pa) , S_w (-), P_c (Pa) , K_w^{int} ($\mathrm{m^2}$) and D_v^{int} ($\mathrm{m^2\,s^{-1}}$) stand respectively for the density of liquid and water vapour, the dynamic viscosity of liquid, the porosity, the molar mass of water, the perfect gas constant, the temperature, the saturated vapour pressure, the liquid saturation degree, the capillary pressure, the intrinsic permeability and diffusivity.

To assess the evolution of saturation degree with regard to relative humidity, the relationship proposed by van Genuchten [44] is used (Eq. 3).

$$S_w=[1+(-\alpha\ln(h_r))^{\gamma}]^{-\beta} \tag{3}$$

$$\gamma=\frac{1}{1-\beta} \tag{4}$$

with α (-), γ (-) and β (-) three parameters that can be fitted on experimental isotherms and h_r (-) the relative humidity. Furthermore, the relation (4) is proposed by van Genuchten to restrict γ values according to β in the case of Mualem pore size distribution [45].

Concerning transport properties, another important point which has to be considered is their evolutions regarding the saturation degree [43]. In order to model these dependencies, the relative permeability is modelled according to van Genuchten [44] model (Eq. 5) and the relative diffusivity is taken as Millington and Quirk [46] suggest (Eq. 6).

$$k_{rl}(S_w) = \frac{K_w^{eff}}{K_w^{int}} = S_w^{n_k}[1 - (1 - S_w^{\frac{1}{\beta}})^{\beta}]^2 \tag{5}$$

$$d_{rl}(S_w) = \frac{D_v^{eff}}{D_v^{int}} = \phi^{a_{mq}}(1 - S_w)^{b_{mq}} \tag{6}$$

where n_k (-) is a pore factor, related to tortuosity, equal to 0.5 according to van Genuchten [44], but evolving in the range of -4.5 to 5.5 (see for instance [47, 48]), and β (-) the factor set in the relation (3), a_{mq} (-) and b_{mq} (-) model parameters taken between 1.3 and 2.74 and 3.3 and 4.2 respectively [43]. Finally, drying flux through boundaries conditions is assumed to be convective and takes the form of equation (7).

$$\boldsymbol{\Phi}_{\text{conv}} = h_c(P_{ci} - P_{ce})\boldsymbol{n} \tag{7}$$

where $\boldsymbol{\Phi}_{\text{conv}}$ is the drying flux ($\mathrm{m\,s^{-1}}$), h_c ($\mathrm{m\,s^{-1}\,Pa^{-1}}$) is the drying boundary coefficient, P_{ci} and P_{ce} in (Pa) are respectively the surface and surrounding capillary pressure and $\boldsymbol{n}$ the normal of the surface. These capillary pressures are determined by the Kelvin-Laplace equation.

2.3. Shrinkage modelling

Drying shrinkage is a macroscopic consequence of the evolution of water content in the porous body. It is a combination of a variation of capillary pressure [49], disjoining pressure [50, 51] and surface free energy upon drying. To model this phenomenon, it exists on the one hand, simple models based on phenomenological observations [52] and on the other hand poro-mechanical approaches [53, 54] (review of poromechanical model in Di Bella et al. [55]). The model used in this application is the one proposed by Coussy et al. [54] (Eq. 8a). They introduce the equivalent pore pressure π (Eq. 8b) that takes into account the contribution of the interface energy $U(S_w)$ (Pa).

$$\boldsymbol{\epsilon}_{ds} = \frac{1-2\nu}{E} b_w \pi \mathbf{1} \tag{8a}$$

$$\pi = P_m - U(S_w) \quad \text{with} \quad U(S_w) = \int_{S_w}^{1} P_c(S_w^{'}) dS_w^{'} \tag{8b}$$

with E (Pa) the young modulus, P_m (Pa) the average pore pressure, which is equal to $P_m = S_w P_c$ in the case where gas pressure is negligible (close to atmospheric pressure) and b_w (-) the Biot liquid coefficient. Finally equation (8a) assumes that the porous body is elastic. This may lead to an underestimation of two or three times the final shrinkage amplitude [56]. To avoid this pitfall, a viscous-elastic modelling is used [57] (Eq. (9)).

$$\epsilon_{ds} = (1-2\nu) b_w S_w \int_{t'=0}^{t'=t} \left(\frac{1}{E} \frac{dP_c}{dt'} + J(t-t', t') \frac{dP_c}{dt'} \right) dt' \tag{9}$$

with J (Pa^{-1}) the specific creep. This model allows for retrieving partially reversible drying shrinkage in the case of wetting [58], but not completely the hysteresis, also present in the water retention curve, but not modelled here.

2.4. Creep modelling

2.4.1. Basic creep

The model used in this work is the one presented by Hilaire [31]. It is a modified Burger model composed in serial of a Kelvin-Voigt solid plus an aging dashpot. The constitutive equations of the model are given by the equations:

$$\dot{\epsilon}_{bc} = \dot{\epsilon}_{kv} + \dot{\epsilon}_{am} \tag{10a}$$

$$\frac{\dot{\sigma}}{k_{kv}} = \tau \ddot{\epsilon}_{kv} + \left(1 + \frac{\dot{k}_{kv}}{k_{kv}} \tau \right) \dot{\epsilon}_{kv} \quad \text{with} \quad \tau = \frac{\eta_{kv}}{k_{kv}} \tag{10b}$$

$$\dot{\epsilon}_{am} = \alpha_{bc} \frac{< \sigma >_+}{\eta_{am}(t)} + \frac{< \sigma >_-}{\eta_{am}(t)} \quad \text{with} \quad \eta_{am}(t) = \eta_{am}^{\infty} \times t \tag{10c}$$

with α_{bc} (-) a parameter allowing to model the dissymmetric behaviour between tension and compression (not investigated in this paper α_{bc} =1, for more information regarding the impact of α_{bc} see [31]), k_{kv} (Pa) the stiffness and η_{kv} ($\mathrm{Pa\,s}^{-1}$)

the dynamic viscosity of the Kelvin-Voigt solid and η_{am}^{∞} ($\mathrm{Pa\,s^{-1}}$) the final dynamic viscosity of the aging dashpot.

To take into account multi-axial loadings, this approach has been classically extended to three-dimensional problems using the behaviour law of the material by introducing the basic creep Poisson's ratio ν_{bc} (Eq. 11) .

$$J_{ijkl}(t,t') = J_{1D}(t,t')\left[-\nu_{bc}\delta_{ij}\delta_{kl} + \frac{1+\nu_{bc}}{2}(\delta_{il}\delta_{jk} + \delta_{ik}\delta_{jl})\right] \tag{11}$$

with $J_{1D}(t,t')$ the basic specific creep in the uniaxial case and δ the Kronecker symbol.

2.4.2. Drying creep

Drying creep is the result of two distinct phenomena. The micro-cracking part which is characterized when the cracking of the material is considered and the stress-induced shrinkage part which has to be explicitly taken into account. Several works [59, 60, 61] highlight the proportionality relationship between drying shrinkage and drying creep strains. This observation leads to a model linking the drying creep strain rate to the drying shrinkage one (Eq. 12).

$$\dot{\boldsymbol{\epsilon}}_{dc} = \lambda_{dc}|\dot{\epsilon}_{ds}|\boldsymbol{\sigma} \tag{12}$$

with λ_{dc} ($\mathrm{Pa^{-1}}$) a constant and σ (Pa) the uniaxial stress. This model is extended in a fully three dimensional problem by introducing a drying creep Poisson's ratio, equal to the basic creep, in a similar way than basic creep (see equation 11).

2.5. Mechanical modelling

2.5.1. Damage modelling

The mechanical model used in this work is an isotropic damage model; the decrease of the material stiffness is described by the evolution of a variable D. In an isotropic case, this scalar variable is introduced in the behaviour law (Eq. 13).

$$\boldsymbol{\sigma} = (1-D)\mathbb{C} : \boldsymbol{\epsilon} \tag{13}$$

with $\mathbb{C}$ the four order stiffness tensor non-damaged. The allowable values of D $\in$ [0;1]. The evolution of the damage depends on a load threshold function: f= ϵ_{eq}-$\kappa(D)$, where κ the hardening-softening parameter is equal to the maximum of ϵ_{eq} or ϵ_{d_0} and ϵ_{d_0} the tensile damage threshold corresponding to $\frac{f_t}{E}$. Classically, the equivalent strain (ϵ_{eq}) is taken as proposed by Mazars [62]:

$$\epsilon_{eq} = \sqrt{\sum_{i=1}^{3} < \epsilon_i >_+^2} \tag{14}$$

with, ϵ_i the principal strains extension. Under multi-axial loading, the damage variable is taken as a linear combination of variables D_t and D_c (Eq. (15)).

$$D = \alpha_t^{\beta_D} D_t + \alpha_c^{\beta_D} D_c \tag{15}$$

with β_D (-) a parameter introduced by Pijaudier-Cabot et al. [63] to describe shear dominated problems. In the following applications this parameter will always be equal to 1. Then α_t parameter is calculated based on the principal strains ϵ_i:

$$\alpha_t = \sum_{i=1}^{3} \frac{\epsilon_i^t < \epsilon_i >_+}{\epsilon_{eq}} \tag{16}$$

with ϵ_i^t positive principal strains and $\alpha_c + \alpha_t = 1$. Regarding compression and tension damages, the original evolution law proposed by Mazars [62] is used (Eq. 17) in compression. In order to use energetic regularization, damage evolution law in tension is defined as Feenstra and De Borst [64] proposed (Eq. 18).

$$D_c = 1 - \frac{\epsilon_{d0}(1 - A_c)}{\kappa} - A_c \exp(-B_c(\kappa - \epsilon_{d0})) \tag{17}$$

$$D_t = 1 - \frac{\epsilon_{d0}}{\kappa} \exp(-B_t(\kappa - \epsilon_{d0})) \tag{18}$$

ϵ_{d0} (-) the damage threshold in tension, A_c (-) and $B_{t,c}$ (-) the model parameters controlling the post-pic phase evolution of the material behaviour.

To avoid mesh dependency and non uniqueness of the solution due to softening behaviour of concrete, an energetic regularization is used [65]. This regularization is based on parameter B_t (-) which is a function of the size of element h (m), the tensile strength f_t (Pa), the fracture energy G_f (J m^{-2}) and the threshold ϵ_{d0} (-):

$$B_t = \frac{h \times f_t}{G_f - \frac{hE\epsilon_{d0}^2}{2}} \tag{19}$$

2.5.2. Effect of h_r on mechanical strength

Drying effects are numerous and occur at different time and scales in cementitious materials. First of all, rather hydration is not investigated, there is an obvious competition between hydration (consumption of water by cement reaction) and drying (exchange between concrete porosity and ambiant atmosphere). As a result moist curing plays an important role in strength development [66]. Second of all, drying shrinkage appears as a macroscopic consequence of drying. As concrete and more generally cementitious material present heterogeneity and low permeability, differential drying shrinkage develops both between the core and the edge of the material [4, 5] as well as between the different components due to stiffness difference [7, 8, 10]. Finally, drying in porous network generates pore pressure composed of capillary pressure, disjoining pressure and surface energy which are involved in the pre-stressing of the solid part of the microstructure. As mentioned by Bažant et al. [2] the latter explain in part the improvement of the tensile strength if concrete is dried without any cracking. These are confirmed by experimental evidences [67, 68, 69] and are modelled in others approaches [28, 29].

To account for the impact of pore pressure in the modelling of the mechanical behaviour, the initial behaviour law (Eq. 13) is expressed in the framework of porous media [70] (Eq. 20).

$$\boldsymbol{\sigma} = \mathbb{C}\boldsymbol{\epsilon} + bp\mathbf{1} \tag{20}$$

with p (Pa) the pore pressure and $\boldsymbol{\sigma}$ (Pa) the total stress. Then the aforementioned f threshold function of the original Mazars's model is conserved but the threshold (ϵ_{d_0}) is rewritten as (Eq. 21).

$$\epsilon_{d_0} = \frac{f_t}{E} - \frac{(1-2\nu)}{E} b_m S_w P_c \quad \text{with} \quad P_c < 0 \tag{21}$$

with b_m (-) a calibration parameter. To illustrate the positive contribution of capillary pressure in the modelling (Eq. 21), the behaviour of an unity cubic volume

under respectively tension (Fig. 1a) and compression (Fig. 1b) loadings, is investigated. In these examples, drying shrinkage is uniform, *i.e.* there is no drying cracks.

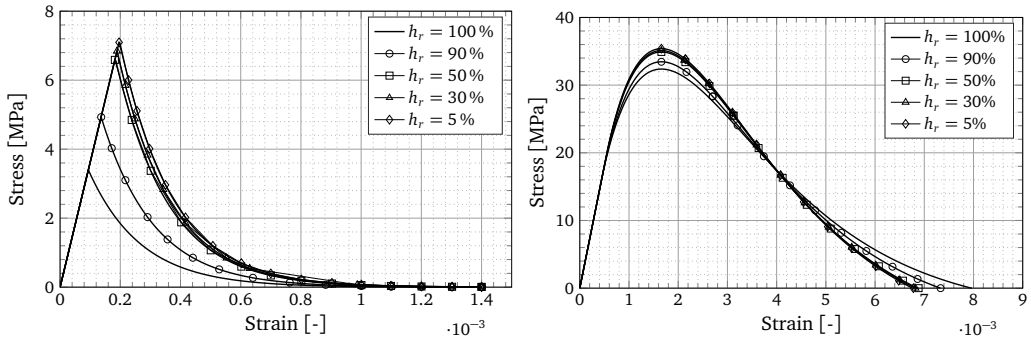

(a) Tensile response (b) Compressive response

Figure 1: Mechanical responses with $b_m = 0.3$ (Eq. 21) for different uniform values of relative humidity (h_r), in tension and in compression (drying shrinkage is thus uniform, *i.e.* no drying cracks occur).

Neither in tension nor in compression the tangent modulus is affected by capillary pressure (Fig. 1). On the contrary, the peak tensile strength is strongly influenced by the saturation degree (Fig. 1a). This is not similar under compression (Fig. 1b). In compression, the extensions are not direct but induced by loading. As a result, the impact of capillary pressure is reduced. Another important point is the non linearity of the impact drying. This results from the function $S_w P_c$ which is an increasing function non linear. Finally, in this first attempt to model the effect of pore pressure, only capillary pressure is taken into account. The pressure induced by disjoining pressure and surface energy are not considered. It mays result in a misleading impact of pore pressure in the low relative humidity ranges (below $h_r = 40\,\%$).

3. Cases of application

The hygro-mechanical approach presented in section 2 is applied to two different cases. The first one is interested in a prismatic specimen that undergoes drying shrinkage until drying equilibrium. The second regards a bending beam subjected to mechanical loading after a curing period of 70 days. The experimental data used

as a basis for this modelling were obtained within the framework of the PhD of Soleilhet [17]. During the PhD no creep data were obtained. To overcome this problem, creep models were identified on VeRCoRs project data [71]. The concretes used in both experimental investigations were almost similar.

3.1. Identification of creep model parameters on VeRCoRs data base

VeRCoRs is a project led by Électricité de France [72]. It consists in a 1/3 scale concrete containment building (CCB) built to improve the understanding and the modelling capabilities of ageing and leakage of double walls CCB. In this project, creep were monitored on cylindrical specimens of 16×100 cm^2 size over a period of 10 months (Fig. 2a). The storage conditions of the specimens were a temperature of 20 °C and a relative humidity of 50 %. Mechanical compression loading of 12 MPa was applied after 90 days. The strains were measured with strain gauges (for more information regarding experimental protocol, see Charpin et al. [73] on another concrete.).

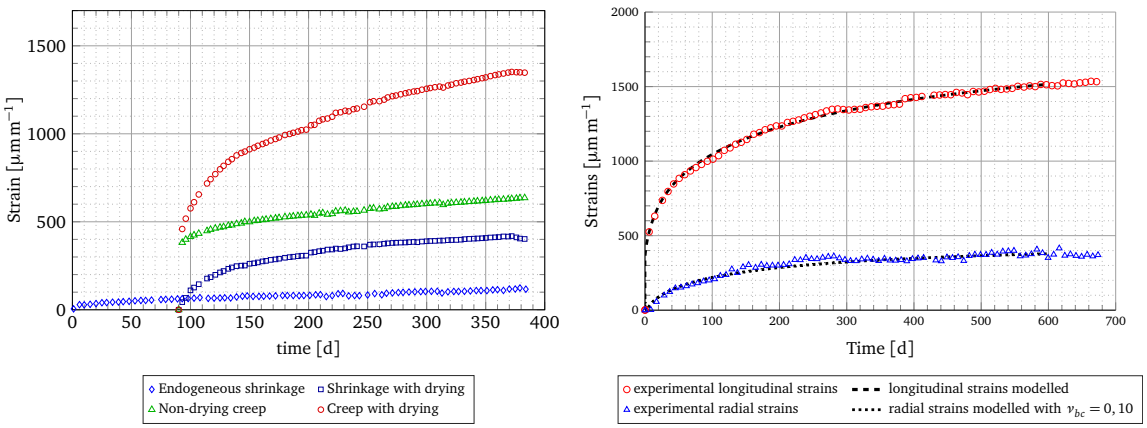

(a) Delayed strains of VeRCoRs concrete [71] (b) Total creep strains identified

Figure 2: Experimental and identified delayed strains of VeRCoRs concrete

Characteristic delayed strains were computed from this data base and then identified in order to simulate the total creep (Fig. 2b). Data regarding delayed strains (basic and drying specific creep) are presented in Appendix C. Identified parameters are summarized in Table 1. In order to fit the radial strains, a creep Poisson ratio of 0.10 is identified.

τ_{am} (d)	η_∞ (GPa s^{-1})	k_{kv} (GPa)	τ_{kv} (d)	ν_{bc} (-)	λ_{dc} (MPa^{-1})
90	130	135	15	0.10	7.82×10^{-2}

Table 1: Set of creep parameters identified on VeRCoRs data

3.2. Drying shrinkage prism

In this application, a $7 \times 7 \times 28$ cm^3 concrete prism is subjected to a dry environment with 45 % of relative humidity for a period of 400 days. The modelling is carried out using a three-dimensional simulation of one eighth of the test piece due to symmetry conditions (Fig. 3).

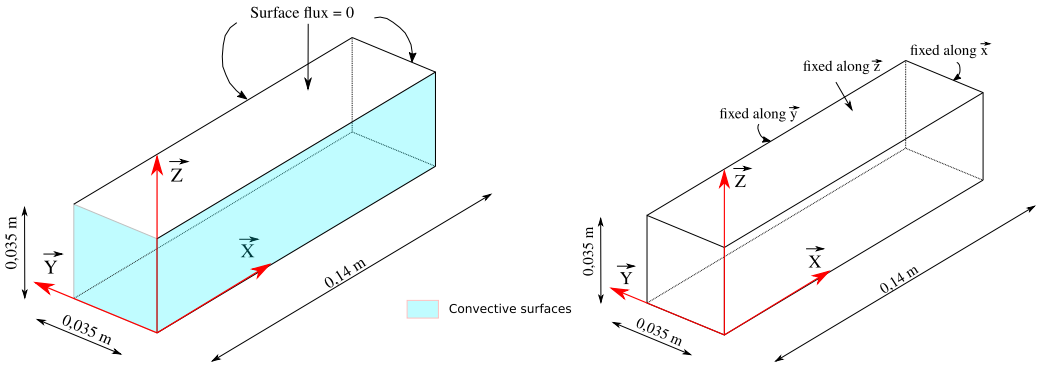

(a) Drying problem (b) Mechanical problem

Figure 3: Geometries and boundaries conditions for drying shrinkage prism.

For drying submodelling, the ambient relative humidity is imposed on convective surfaces (Fig. 3a). The parameters of the drying model (Tab.2) are identified based on the relative mass variation of the experimental specimens (Fig. 4a). To assess the evolution of relative mass variation, the equation (22) is used.

$$w_n = \frac{\phi \rho_w}{\rho_c} S_w \tag{22}$$

with w_n (%) the water mass content, ρ_c (kg m^{-3}) the satured concrete density. This relationship allows to compare the computed mass variation with the experimental results and to identified drying parameters (Tab. 2). The drying identification was processed algorithmically by an automatic update of the finite element model parameters (see Carette et al. [74]).

β (-)	α (-)	n_k (-)	K_w^{int} (m^2)	ϕ (-)	h_c ($m\,s^{-1}\,Pa^{-1}$)	ρ_c ($kg\,m^{-3}$)
0.48	5.6	-0.30	3.88×10^{-21}	0.17	48	2370

Table 2: Identified set of drying parameters. For lack of sensitivity in this hydric condition water vapour diffusion parameters are taken equal to a_{mq}= 2.74, b_{mq}= 4.2 and $D_v^{int} = 2.55 \times 10^{-5}\ m^2\,s^{-1}$ as suggested by Thiery et al. [43].

Drying equilibrium (close to 5.2 % after 400 days) and drying kinetic are well modelled (Fig. 4a). The accurate prediction of the relative mass variation allows to model the drying shrinkage according to the equation (9). For mechanical modelling, the symmetry plans of the sample are blocked (Fig. 3b). The resulting evolution with an identify value of Biot parameter equal to 0.30, overestimates the ultimate shrinkage at equilibrium of about 18 % (Fig. 4b). In addition, it is remarkable that the model does not seem at equilibrium at 400 days even if relative mass variation is constant. This is probably due to the visco-elastic part of the model. In this case, the model is not totally in accordance with experimental data. However, it allows to stay in a poromechanic framework for drying shrinkage and effect of capillary pressure on strength.

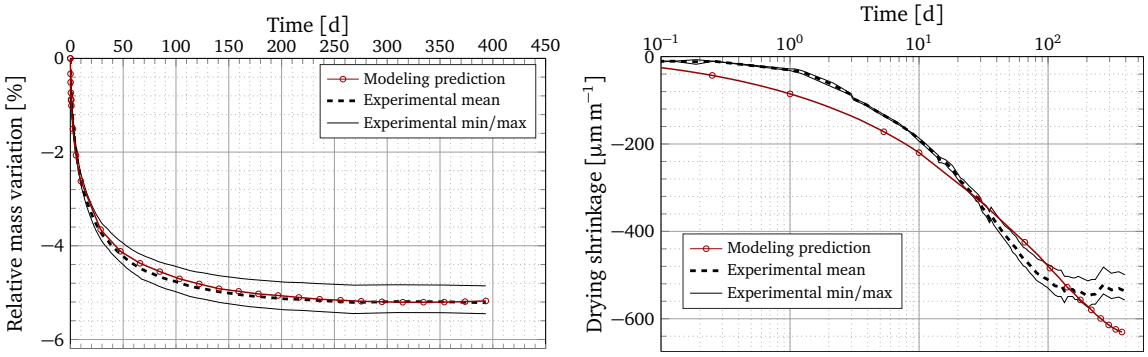

(a) Prediction of relative mass variation

(b) Prediction of drying shrinkage

Figure 4: Evolution of drying and shrinkage over 400 days

According to the evolution of shrinkage, the normal stress state (along the x axis) is studied (Fig. 5). Three modelling scenarios are investigated:

1. One without creep;
2. A second with creep taken into account ;

3. A third with creep and capillary pressure.

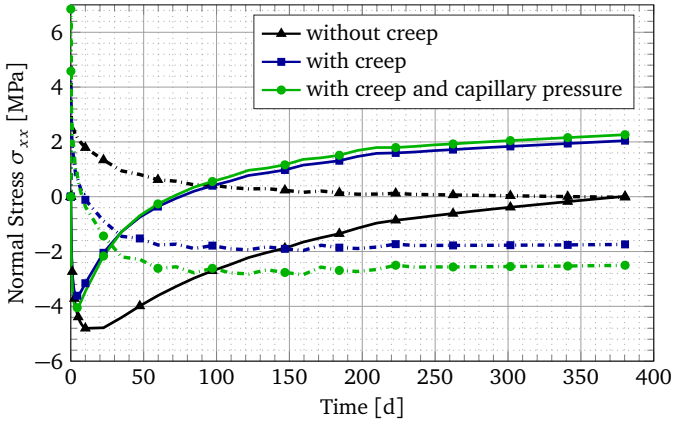

Figure 5: Evolution of σ_{xx} (see Fig. 3) on the surface in dotted lines and in the core of the test piece in solid lines.

Influence of creep on the evolution of normal stress (σ_{xx}) is highlighted. For the three models, the samples are free of stresses at time zero. With drying, the normal stress reaches the tensile strength at the edge. Different scenarios are simulated. Regarding the edge stresses, in the case (1), they soften until the damage variable reached the value of 1. Conversely in the case (2), the stress decreases rapidly due to relaxation phenomena within the specimen. Similarly, the compressive stress reached in the core of the specimen is 20 % greater in the case (1). In addition, the amount of time needed to inverse the type of loading (tensile ⇔ compressive) is greater without creep (almost 375 days) than with creep (close to 30 days). Finally, the modelling (2) and (3) are almost similar both on the edge and on the core parts. The main difference is located in the peak stress reached on the skin of the sample. With the proposed formulation, the damage threshold is increased and as a result, the material stiffens and the maximum stress reached in the skin of the specimen (almost 7 MPa) increases and limits the evolution of damage.

3.3. Bending test under drying

In the latter application, $10\times10\times84$ cm^3 test specimens (notched and unnotched) are subjected to a drying environment of respectively 30 % and 45 % relative humidity for a period of 70 days. They are then tested in three-points bending test.

Furthermore, experimental data from companion samples, that were kept under water over the same period are available to calibrate mechanical models.

3.3.1. Drying submodelling

The first stage of the numerical modelling is conducted through a three dimensional modelling of the test specimens. Symmetries are not taken into account in order to let open the possibility to use random fields. The mesh of the sample is made of 36400 cubic linear elements. The mesh density is higher on the edge of the sample. These zones are expected to present the strongest drying gradient and a finer mesh (smallest element 1/10 the size of the biggest 20 mm) is necessary. The 70 days of drying are discretized in time as follows: 40 time steps of 45 s followed by 40 time steps of 2115 s, 20 time steps of 8640 s, 20 time steps of 30 240 s, 10 time steps of 216 380 s and finally 10 time steps of 302 780 s. Ambient conditions are applied over the entire external surface through a drying flux. As mentioned previously, drying parameters are identified algorithmically and identified parameters are summarized in the Table 3.

h_r (%)	β (-)	α (-)	n_k (-)	K_w^{int} (m^2)	ϕ (-)	ρ_c ($kg\,m^{-3}$)
30	0.48	5.6	-2.45	1.6×10^{-21}	0.15	2450
45	0.48	5.6	-2.89	0.6×10^{-21}	0.14	2468

Table 3: Sets of drying parameters identified for the beam problem. Density and porosity are characterized experimentally and diffusion parameters remain identical (*i.e* a_{mq}= 2.74, b_{mq}= 4.2 and $D_v^{int} = 2.55 \times 10^{-5}\ m^2\,s^{-1}$).

Regarding the identified drying parameters values, slight differences between the two h_r conditions are noticeable. This can be partially explained by the variability of concrete itself and by the inherent variability between concrete batches. Nevertheless, the parameters are really close.

As previously illustrated, the prediction of the relative mass variation is really accurate (Fig. 6a). Kinetic is well modelled in both condition and the identified value of intrinsic permeability is estimated close to 10^{-21} m^2. This is consistent for ordinary concrete [75].

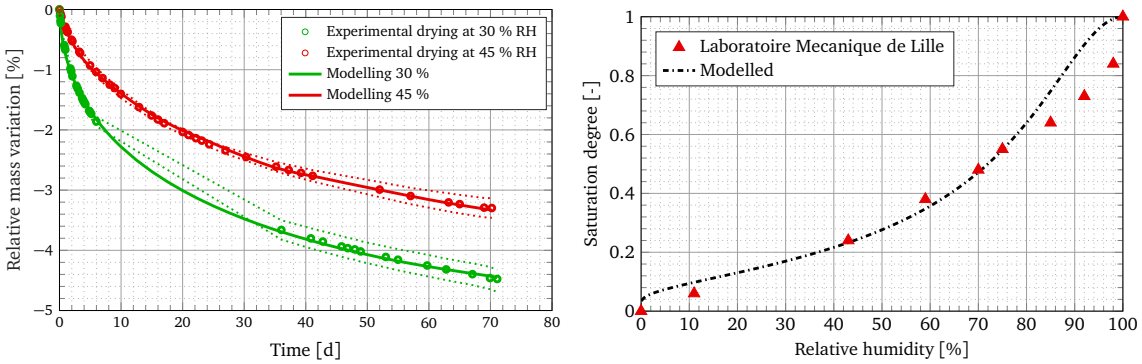

(a) Relative mass variation until mechanical test (b) Modelling versus experimental desorption isotherm

Figure 6: Macroscopic drying properties. Green color for h_r equals to 30 % and red color for 45 %

Another key point in the drying modelling is the assessment of drying fields. This is a difficult task as there is no straight forward method to measure these fields and therefore to validate the modelling. As an attempt to validate drying modelling, the evolution of relative humidity field is plotted (Fig. 7). Since the drying boundaries conditions are symmetric, the resulting fields is as well. The slowness of the process is also illustrated: only few millimeters desaturated after one day (Fig. 7a). Afterwards drying process goes on and applied drying condition ($h_r = 45\,\%$) is reached on the edge of the sample at the end of the modelling period. After 70 days, the center of the specimen is close to 90 % of relative humidity, almost the same as the initial value (98 %). Finally, after 70 days, the drying gradients are important within the specimen. As an illustration, the average humidity gradient between the center and the edge of the sample ($\nabla h_r|_{x=0.42m}$) is almost equal to $1142\,\%\,\mathrm{m}^{-1}$.

3.3.2. Mechanical submodelling

In the mechanical part, the internal stresses induced by drying gradients and the residual mechanical behaviour are determined. The mechanical submodelling is based on the same mesh. Model's mechanical parameters are identified (algorithmically) on experimental data (compressive and bending test) obtained on materials that have been prevented from drying. These tests were performed at the same time (t=70 days) in order to minimize the impact of hydration (Fig. 8). Identified parameters are resumed in Table 4. The first four parameters are identified on the

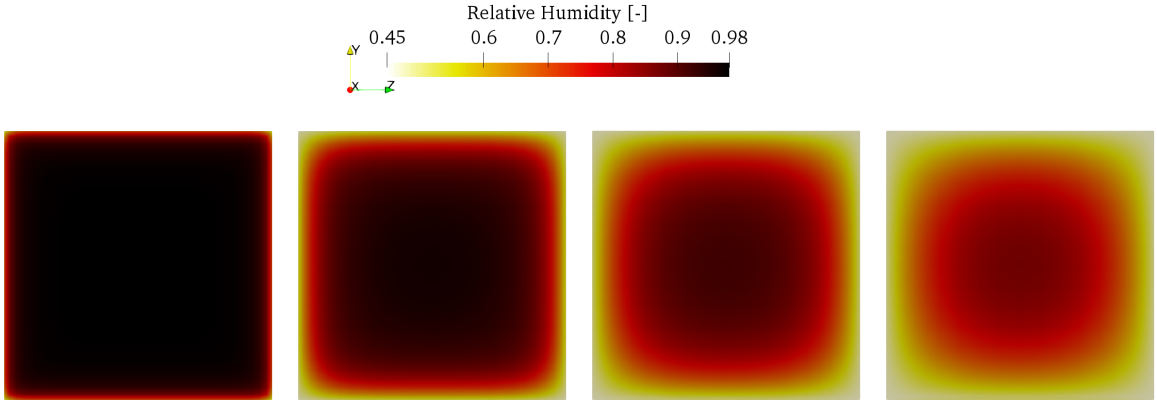

(a) 1 day (b) 10 days (c) 30 days (d) 70 days

Figure 7: Evolution of h_r fields in the middle crossing section. Case of applied $h_r = 45\,\%$

compressive tests. The tensile strength and cracking energy are then identified on the bending tests. Compressive parameters are adjusted if necessary (variation of few percent). It can be seen that the Young modulus values are close between the different modelling. As far as tensile strengths are concerned, they are between 2 and 3 MPa. Finally, the cracking energy is close to $83\,\mathrm{J\,m^{-2}}$ on average. These identified values seem consistent for this type of concrete.

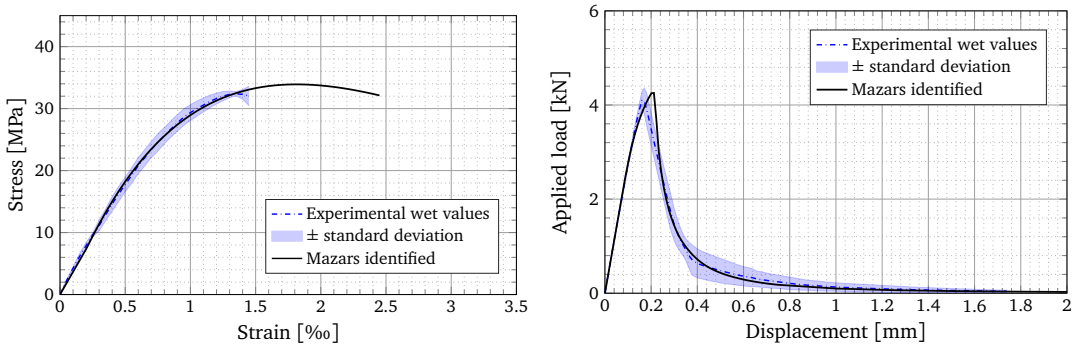

(a) Compression test identified (b) Three points bend test unnotched identified

Figure 8: Mazars model identified. Example of companion samples from ambiance h_r=30 %.

Drying shrinkage is modelled with the same Biot coefficient than the one used in the first application (*i.e* b_w=0.30). At 70 days the predicted value of drying shrinkage is consistent with the experimental value (Fig. 4b). Except for rigid bodies which are locked, the specimen is free to deform. The time stepping of the modelling is the same as the drying submodelling.

Campaign	Test	E (GPa)	ν (-)	a_{comp} (-)	b_{comp} (-)	f_t (MPa)	G_f ($\mathrm{J\,m^{-2}}$)	β_D (-)
	Compressive	36.9	0.24	1.33	1682	3.5	73	1
1	Unnotched Bending	37.1	0.24	1.33	1682	2.5	88	1
	Notched Bending	38.0	0.24	1.33	1682	2.0	73	1
	Compressive	36.7	0.24	1.38	1777	3.4	75	1
2	Unnotched Bending	37.1	0.24	1.38	1777	2.9	95	1
	Notched Bending	38.0	0.24	1.38	1777	2.1	75	1

Table 4: Set of mechanical parameters of Mazars model. Poisson ratio set arbitrarily to ordinary value.

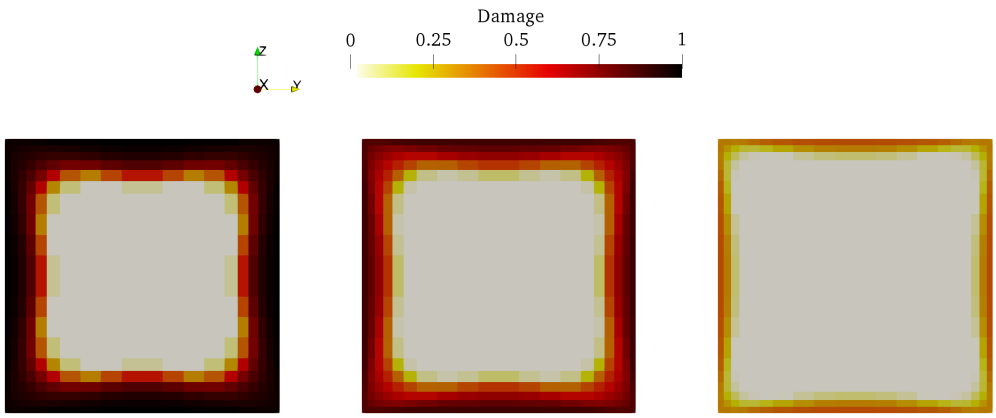

(a) (b) (c)

Figure 9: Damage fields in the middle cross section after 70 days as a function of mechanism modelled: a) only shrinkage b) creep taken into account c) Creep and capillary pressure modelled.

As illustrated (Fig. 5), the decrease in stress within the material is related to the relaxation mechanism and so related to creep. In the case of damage, creep is important but damage threshold is another key parameter which impacts directly the state of damage (Fig. 9). Indeed, the damaged depth is lower when the relaxation is modelled but it is still important. In the proposed model, the modelling of capillary pressure induces an increase of tensile strength. This leads to a significant reduction of damage (Fig. 9c). Here, damage induced by drying impacts only a few millimeters (the damage variable is greater than 0.25 at a depth value of 3.2 mm). In similar conditions (CEM I with a w/c = 0.5 under respectively 33 % and 55 % relative humidy) Wu et al. [76] measured a damage depth close to 4 mm. In addition, the internal stresses are investigated (Fig. 10). Prior to mechanical loading (t=70 days), the stress state is different from zero. The edge are in tensile state and the core is

compressed. This mechanical state evolves with drying and so does the residual mechanical behaviour.

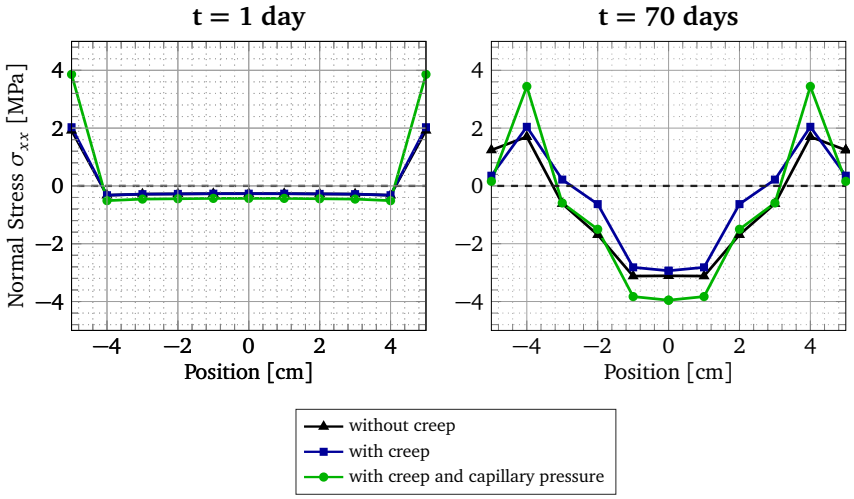

Figure 10: Normal stress along the center line in the middle cross section (x=0.42 m).

For the modelling of the bending tensile test, the mechanical state of the beam (damage, stress and displacement) induced by drying prior to loading is taken into account. At this stage, initial mesh is separated into two meshes. One for the unnotched beam with the same mesh characteristics and another for the notched beam. For this test, the only difference is the removal of the mesh elements in the notch. This result in a mesh composed of 36280 cubic linear elements (Fig. 11).

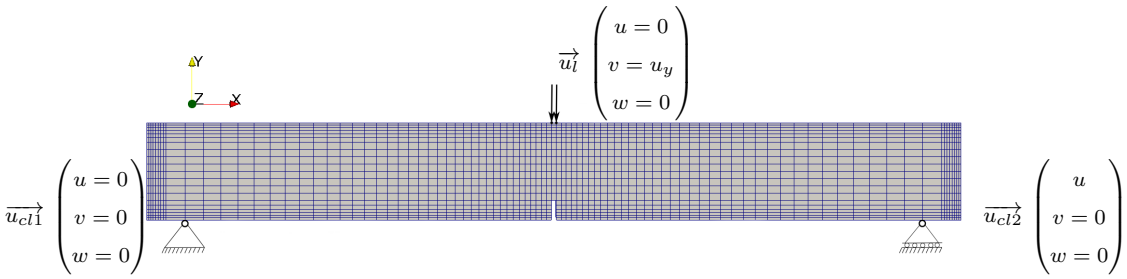

Figure 11: Meshes of bending test: special case of the notched beam. Drying occurs by all the external surfaces for the dried specimens. u_y is the imposed mechanical displacement.

Mechanical boundary conditions are similar in both bending tests. The translation along $\vec{y}$ and $\vec{z}$ are fixed at the supports and the translation along $\vec{x}$ is locked on one of the two supports and only (Fig. 11). The time steps are composed of 123 time steps. They are divided into 3 time steps of 0.67 s followed by 5 time steps

of 2.2 s, 25 time steps of 1.80 s, 25 time steps of 9.28 s, 25 time steps of 17.4 s and finally 40 time steps of 16.9 s.

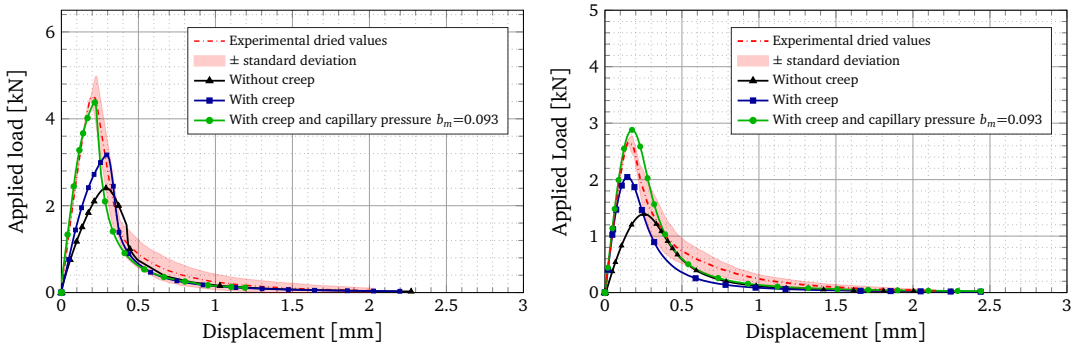

(a) Unnotched beam (h_r = 45 %) (b) Notched beam (h_r = 45 %)

Figure 12: Prediction of the beam behaviour under three points bending load after 70 days of drying. Experimental value obtained on the mean of three samples.

To model the impact of capillary pressure on strength, the value of b_m=0.09 is calibrated on one beam (Fig. 12a) and is no longer modified. Similarly of previous study the predicted mechanical behaviour of the beam is determined regarding the diverse mechanisms modelled (Fig. 12). As expected, the residual macroscopic mechanical behaviour is strongly correlated to the damage state. Taking into account the only mechanism related to drying shrinkage is not sufficient. The stiffness as well as the peak strength are reduced (respectively 50 % and 47 % of peak strength). However, modelling creep improves the behaviour but it is not enough. The gap remains significant in strength (underestimation of 28 % and 23 % of peak strength) even though the stiffness in the notched case is well predicted as opposite of the unnotched case. This difference is explained by the notch. In the case of the specimen unnotched, the edges of the sample are damaged. In contrary in the notched case, as the notch is realised just prior to bending, the partially damaged zone is removed. When the loading is applied, the material in the notch is undamaged. Finally, the modelling of the three mechanisms allows to recover the experimental behaviour both the stiffness and the peak strength.

The behaviour prediction of the samples kept at 30 % relative humidity is then realised (Fig. 13). Except for the modelling of notched specimens, which slightly

underestimates the value of peak strength of 14 % (Fig. 13b), the chosen value is able to stand for the physic of all these tests.

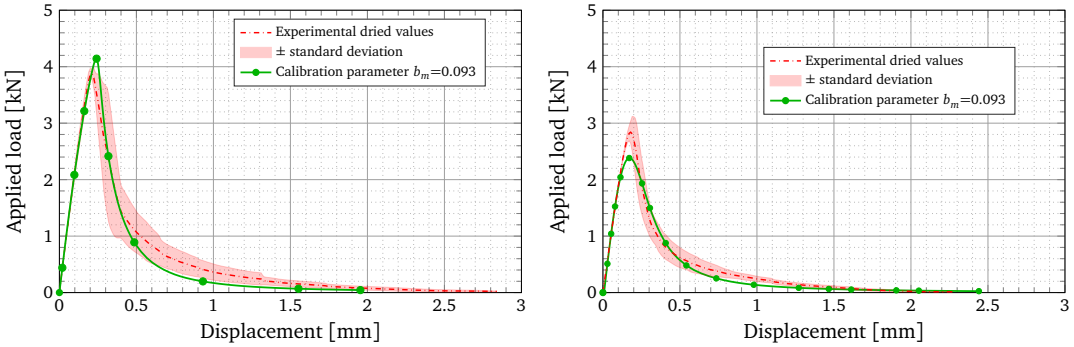

(a) Unnotched beam (h_r = 30 %) (b) Notched beam (h_r = 30 %)

Figure 13: Prediction of the beam behaviour under three points bending load after 70 days of drying. Case of samples at h_r = 30 %.

Finally, the parameter b_m calibrated on mechanical results is more or less related to the Biot coefficient (b_w). The coefficient (b_w) is assumed to be equal to 0.24 for a fully hydrated concrete and may rise to 0.32 for a material hydrated at only 90 % according to the work of Souyris [77]. Even if the ultimate drying shrinkage value is a little bit overestimated (*c.f.* Fig. 4b) the identified value of b_w=0.30 seems consistent. However, if this coefficient is taken into account to model the impact of capillary pressure on strength with the proposed formulation, the experimental curves are poorly reproduced (Fig. 14). Biot coefficient overestimates the peak force of the beams (respectively 39 % for unnotched beam and 52 % for notched beam in the case of h_r =45 % and 42 % in the case of h_r =30 %). The Biot parameter, which induces shrinkage, seems to be more related to macroscopic behaviour whereas the value identified (b_m), three times smaller, seems to be more related to local behaviour of the material. Thus this parameter is related to the damage variable [78] as well as the saturation degree. This statement is also highlighted by the difference between notched beams respectively at h_r = 45 % and h_r = 30 % (Fig. 14b and 14c). The experimental behaviour is almost similar but the modelling predictions are rather different due to different damage state and hydric fields. This observation leads authors such as Sellier et al. [29] to implement models that rely on the state of

stresses to determine this parameter. Furthermore, in the proposed formulation, the equivalent pore pressure (π in part 2.3) does not consider the effects associated to disjoining pressure and surface tension which are predominant in fine pore [78, 79].

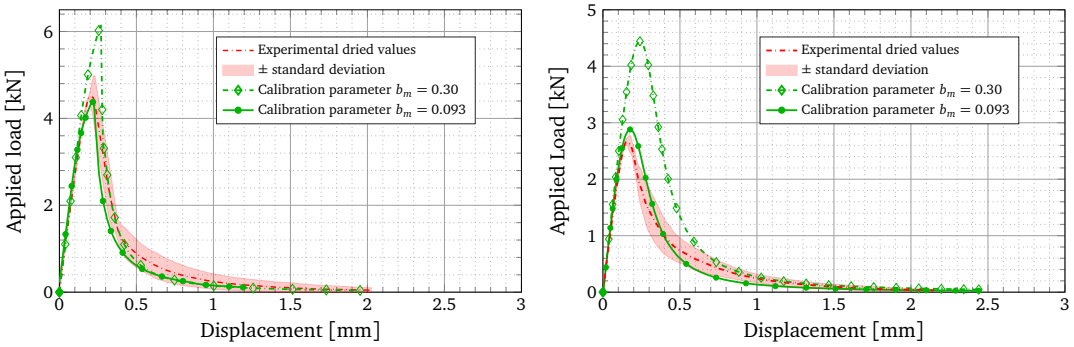

(a) Unnotched beam ($h_r = 45\,\%$)

(b) Notched beam ($h_r = 45\,\%$)

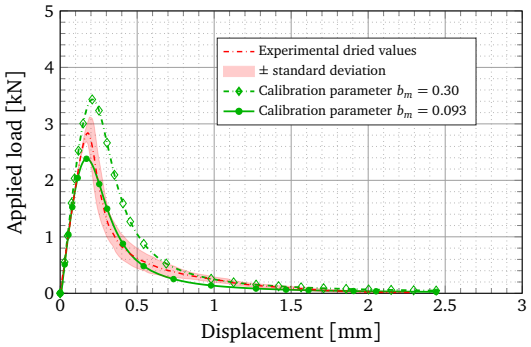

(c) Notched beam ($h_r = 30\,\%$)

Figure 14: Influence of b_m parameter on mechanical behaviour

4. Conclusion

The main goal of this study was to extend a Chemo-Thermo-Hygro-Mechanical model previously initiated by Benboudjema and Torrenti [23] continued by Briffaut et al. [30], completed by Hilaire et al. [31] and improved with the incorporation of the effect pore pressure on mechanical strength on a poromechanical framework. This multi-physics model was reduced at the only hygro-mechanical part in order to model the impact of drying on cracking and mechanical behaviour of a mature concrete in an isothermal conditions. To pursuit this goal, a sequential analysis has been developed. It was composed of a first stage of modelling drying transfers through

a diffusion equation that considered liquid permeation and water vapour diffusion terms. It was followed by a modelling of the drying shrinkage by a poromechanical model with capillary pressure as a driving force. The basic creep strains were modelled by a simple four parameters rheological model and the additional strains due to drying creep were modelled. The mechanical model used was a classic damage model regulated in cracking energy. This mechanical model was thus modified to account for the impact of capillary pressure on strength. The model was applied on two different cases. One on a prism subjected to 400 days of drying and a second on beams kept in dry atmosphere and then brought to failure by mechanical loading. The following conclusions can be drawn from the work presented:

- To model the impact of drying on mechanical behaviour, the modelling of only drying shrinkage was not sufficient. This led to a significant underestimation of the residual mechanical behaviour (around 50 % in the case of 45 % relative humidity). Stress relaxation induced by creep was necessary and it reduced the underestimation to 25 %. Finally, the consideration of capillary pressure in the mechanical behaviour allowed to approach the real behaviour of the material with a weaker cracking induced shrinkage.

- The prediction of the behaviour of bending specimens under mechanical loading after drying was consistent with the experimental behaviour. Thus by calibrating the parameters on one of the tests it was possible to simulate the other experimental tests in a suitable way, keeping the same set of parameters.

- In the proposed modelling, capillary pressure was used as a driving force to model drying shrinkage. It also allows to model the positive effect of capillary suction. Thus, to account for the drying shrinkage and the positive effect induced by capillary suction, the use of the same Biot coefficient, was not possible. In our modelling two different values were used (respectively $b_w = 0.30$ and $b_m = 0.093$) to avoid an overestimation of 45 % in average of the mechanical behaviour.

In an attempt to extend this study, some prospects of improvement can be investigated. Among these, the heterogeneity of the material is an important factor. It

will be interesting to model heterogeneities to consider the interfacial transition zone (ITZ). This area known to show cracking due to strains incompatibilities between the components, will change the macroscopic mechanical behaviour of the material. So far, this phenomenon is not modelled. In addition, cracking is a discontinuous phenomenon and the modelling presented here is continuous. This approach can be questioned by comparing it to a discrete model. Work in this direction is currently ongoing. They will provide more realistic cracking surfaces. Finally, the last point to investigate concerns the Biot coefficient. It would be interesting to see how the latter evolves according to parameters such as geometry, the severity of drying conditions or mechanical loading and damage.

Appendix A. Mix proportion

To maximise the effect of drying shrinkage, the material used in this study is an ordinary concrete with a high water to cement ratio (w/c= 0.62). The mix proportions of each component are given in the table A.5. The concrete is made with Ordinary Portland Cement and a plasticizer is added. Aggregates are limestone aggregates. Its usual mechanical characteristics are: an average compressive strength at 28 days of 40.6 MPa and a tensile strength obtained by splitting test of 3.5 MPa both on 16×32 cm^2 cylinders.

Coumpound	Nature	Quantity	Unit
Cement	CEM I 52,5 R	320	$\mathrm{kg\,m^{-3}}$
Sand	Siliceous	830	$\mathrm{kg\,m^{-3}}$
Aggregate (4-11mm)	Limestone	445	$\mathrm{kg\,m^{-3}}$
Aggregate (8-16mm)	Limestone	550	$\mathrm{kg\,m^{-3}}$
Water (total)		197.6	$\mathrm{kg\,m^{-3}}$
Plasticizer	SIKAPLAST Techno 80	2.75	$\mathrm{kg\,m^{-3}}$

Table A.5: Concrete mix parameters

Appendix B. Numerical flow chart

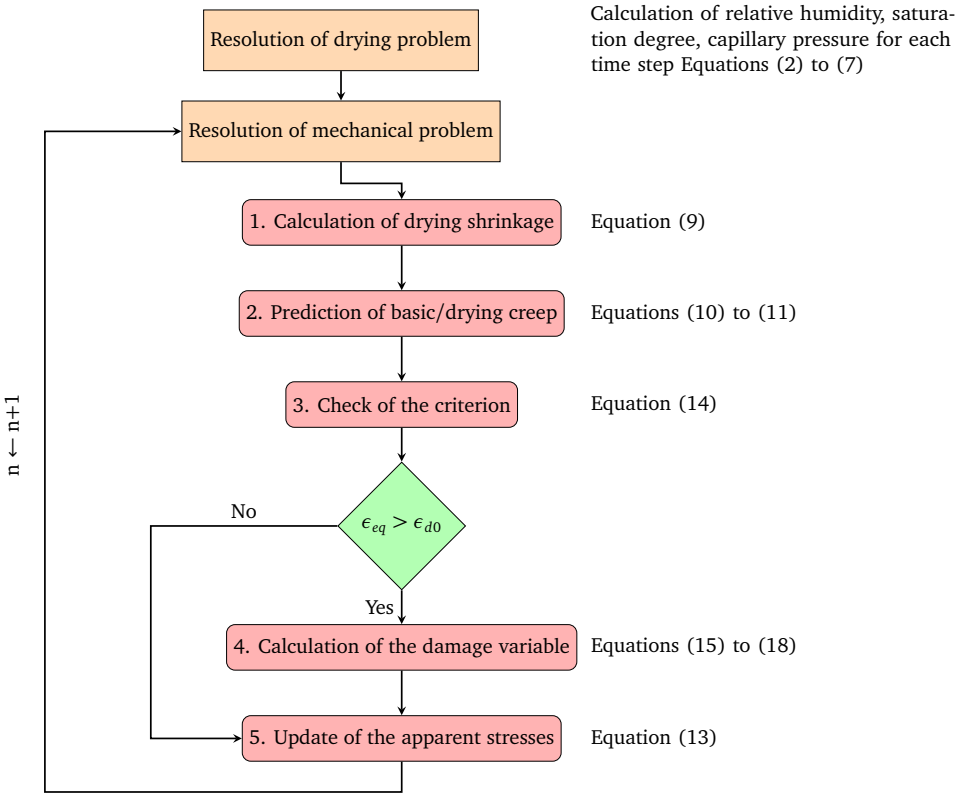

Figure B.15: Flow chart of the hygro-mechanical model

Appendix C. Creep data

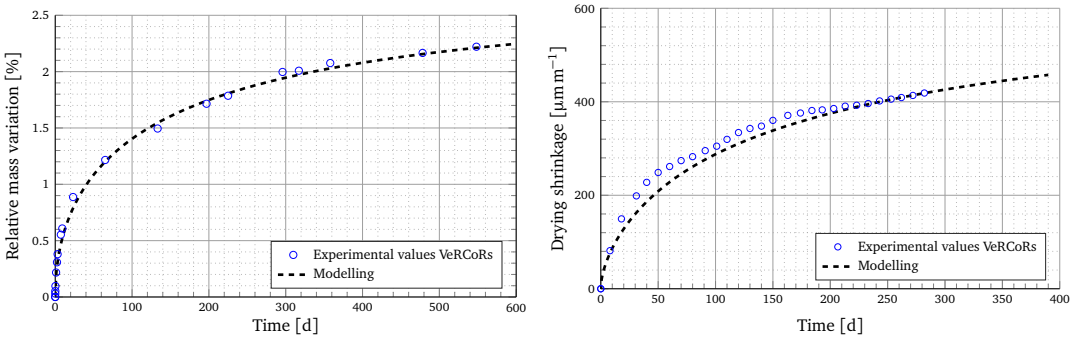

(a) Drying of 16×100cm^2 (b) Drying creep

Figure C.16: Drying and drying shrinkage from VeRCoRs project

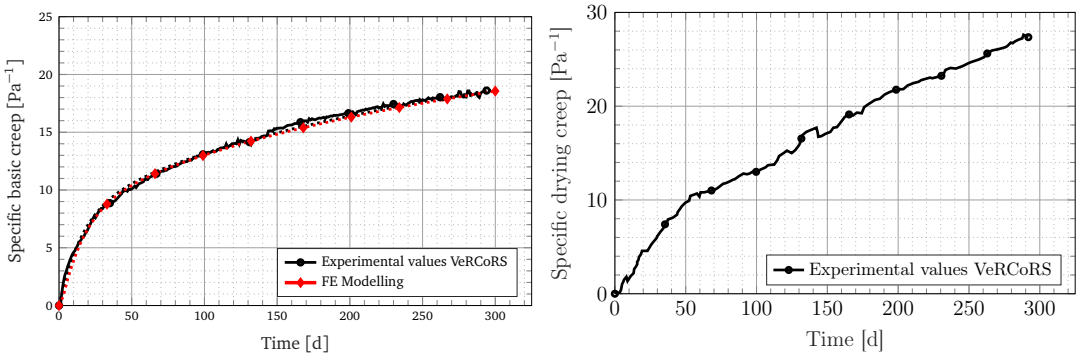

(a) Specific basic creep

(b) Specific drying creep

Figure C.17: Creep data from VeRCoRs project

References

[1] G. Ranzi, R. I. Gilbert, Time-dependent behaviour of concrete structures, CRC Press, 2010.

[2] Z. P. Bažant, A. B. Hauggaard, S. Baweja, F.-J. Ulm, Microprestress-solidification theory for concrete creep. i: Aging and drying effects, Journal of Engineering Mechanics 123 (1997) 1188–1194.

[3] J. Brooks, 10 - Creep of Concrete, in: J. Brooks (Ed.), Concrete and Masonry Movements, Butterworth-Heinemann, 2015, pp. 281–348.

[4] Z. P. Bažant, F. H. Wittmann, Creep and shrinkage in concrete structures, number 405 in Numerical Methods in Engineering, Wiley New York, 1982.

[5] I. Yurtdas, H. Peng, N. Burlion, F. Skoczylas, Influences of water by cement ratio on mechanical properties of mortars submitted to drying, Cement and Concrete Research 36 (2006) 1286–1293.

[6] A. Michou, A. Hilaire, F. Benboudjema, G. Nahas, P. Wyniecki, Y. Berthaud, Reinforcement-concrete bond behavior: experimentation in drying conditions and meso-scale modeling, Engineering Structures 101 (2015) 570582.

[7] J. Bisschop, J. Van Mier, Effect of aggregates on drying shrinkage microcracking in cement-based composites, Materials and Structures 35 (2002) 453–461.

[8] F. Lagier, X. Jourdain, C. D. Sa, F. Benboudjema, J. Colliat, Numerical strategies for prediction of drying cracks in heterogeneous materials: Comparison upon experimental results, Engineering Structures 33 (2011) 920 – 931.

[9] A. Idiart, J. Bisschop, A. Caballero, P. Lura, A numerical and experimental study of aggregate-induced shrinkage cracking in cementitious composites, Cement and Concrete Research 42 (2012) 272 – 281.

[10] Y. Chen, J. Wei, H. Huang, W. Jin, Q. Yu, Application of 3d-dic to characterize the effect of aggregate size and volume on non-uniform shrinkage strain distribution in concrete, Cement and Concrete Composites 86 (2018) 178–189.

[11] W. J. Weiss, W. Yang, S. P. Shah, Shrinkage cracking of restrained concrete slabs, Journal of Engineering Mechanics 124 (1998) 765774.

[12] T. Mauroux, F. Benboudjema, P. Turcry, A. At-Mokhtar, D. O., Study of cracking due to drying in coating mortars by digital image correlation, Cement and Concrete Research 42 (2012) 10141023.

[13] I. Maruyama, Y. Nishioka, G. Igarashi, K. Matsui, Microstructural and bulk property changes in hardened cement paste during the first drying process, Cement and Concrete Research 58 (2014) 20 – 34.

[14] N. Burlion, F. Bourgeois, J.-F. Shao, Effects of desiccation on mechanical behaviour of concrete, Cement and Concrete Composites 27 (2005) 367–379.

[15] S. Pihlajavaara, A review of some of the main results of a research on the ageing phenomena of concrete: Effect of moisture conditions on strength, shrinkage and creep of mature concrete, Cement and Concrete Research 4 (1974) 761–771.

[16] I. Maruyama, H. Sasano, Y. Nishioka, G. Igarashi, Strength and young's modulus change in concrete due to long-term drying and heating up to 90 °C, Cement and Concrete Research 66 (2014) 48 – 63.

[17] F. Soleilhet, Étude expérimentales et numériques des matériaux cimentaires sous sollicitations hydro-mécaniques., Ph.D. thesis, Université Paris-Saclay, 2018.

[18] H. Sasano, I. Maruyama, A. Nakamura, Y. Yamamoto, M. Teshigawara, Impact of drying on structural performance of reinforced concrete shear walls, Journal of Advanced Concrete Technology 16 (2018) 210–232.

[19] A. Abbas, M. Carcasses, J. P. Ollivier, Gas permeability of concrete in relation to its degree of saturation, Materials and Structures 32 (1999) 3–8.

[20] N. Burlion, I. Yurtdas, F. Skoczylas, Comportement mécanique et séchage de matériaux à matrice cimentaire: Comparaison mortier/béton, Revue française de génie civil 7 (2003) 145–165.

[21] M. C. fib, Code-type models for structural behaviour of concrete, State-of-Art-Report, fib – International Federation for Structural Concrete, 2013.

[22] N. EN, 1-1:"eurocode 2: Calcul des structures en béton-partie 1-1: règles générales et règles pour les bâtiments", 2005.

[23] F. Benboudjema, J. Torrenti, Early-age behaviour of concrete nuclear containments, Nuclear Engineering and Design 238 (2008) 2495 – 2506.

[24] M. Azenha, C. Sousa, R. Faria, A. Neves, Thermo–hygro–mechanical modelling of self-induced stresses during the service life of RC structures, Engineering Structures 33 (2011) 3442–3453.

[25] G. D. Luzio, G. Cusatis, Solidification - microprestress - microplane (smm) theory for concrete at early age: Theory, validation and application, International Journal of Solids and Structures 50 (2013) 957 – 975.

[26] J. E. Bolander, S. Berton, Simulation of shrinkage induced cracking in cement composite overlays, Cement and Concrete Composites 26 (2004) 861–871.

[27] P. Grassl, H. S. Wong, N. R. Buenfeld, Influence of aggregate size and volume fraction on shrinkage induced micro-cracking of concrete and mortar, Cement and Concrete Research 40 (2010) 85–93.

[28] S. Grasberger, G. Meschke, Thermo-hygro-mechanical degradation of concrete: From coupled 3D material modelling to durability-oriented multifield structural analyses, Materials and Structures 37 (2004) 244–256.

[29] A. Sellier, S. Multon, L. Buffo-Lacarrière, T. Vidal, X. Bourbon, G. Camps, Concrete creep modelling for structural applications: non-linearity, multi-axiality, hydration, temperature and drying effects, Cement and Concrete Research 79 (2016) 301 – 315.

[30] M. Briffaut, F. Benboudjema, J.-M. Torrenti, G. Nahas, Concrete early age basic creep: Experiments and test of rheological modelling approaches, Construction and Building Materials 36 (2012) 373 – 380.

[31] A. Hilaire, F. Benboudjema, A. Darquennes, Y. Berthaud, G. Nahas, Modeling basic creep in concrete at early-age under compressive and tensile loading, Nuclear Engineering and Design 269 (2014) 222 – 230.

[32] CEA, http://www-cast3m.cea.fr, 2018.

[33] X. Jourdain, J.-B. Colliat, C. De Sa, F. Benboudjema, F. Gatuingt, Upscaling permeability for fractured concrete: meso-macro numerical approach coupled to strong discontinuities, International Journal for Numerical and Analytical Methods in Geomechanics 38 (2014) 536–550.

[34] S. Bažant, Zdeněk Pand Sener, J.-K. Kim, Effect of cracking on drying permeability and diffusivity of concrete, ACI Materials Journal 84 (1987) 351–357.

[35] de Sa, C. , Benboudjema, F., Thiery, M. and Sicard, J., Analysis of microcracking induced by differential drying shrinkage, Cement and Concrete Composites 30 (2008) 947 – 956.

[36] M. Asali, B. Capra, J. Mazars, J. Colliat, Numerical strategy for forecasting the leakage rate of inner containments in double-wall nuclear reactor buildings, Journal of Advanced Concrete Technology 14 (2016) 408–420.

[37] Z. P. Bažant, L. Najjar, Drying of concrete as a nonlinear diffusion problem, Cement and Concrete Research 1 (1971) 461–473.

[38] N. Jafarifar, K. Pilakoutas, T. Bennett, Moisture transport and drying shrinkage properties of steel–fibre-reinforced-concrete, Construction and Building Materials 73 (2014) 41–50.

[39] Y. Huang, H. Ye, C. Fu, N. Jin, Modeling moisture transport at the surface layer of fatigue-damaged concrete, Construction and Building Materials 151 (2017) 196 – 207.

[40] Y. Xi, Z. P. Bažant, L. Molina, H. M. Jennings, Moisture diffusion in cementitious materials moisture capacity and diffusivity, Advanced Cement Based Materials 1 (1994) 258–266.

[41] M. Mainguy, O. Coussy, V. Baroghel-Bouny, Role of air pressure in drying of weakly permeable materials, Journal of Engineering Mechanics 127 (2001) 582–592.

[42] O. Coussy, V. Baroghel-Bouny, P. Dangla, M. Mainguy, Evaluation de la perméabilité à l'eau liquide des bétons à partir de leur perte de masse durant le séchage, Revue française de génie civil 5 (2001) 269–284.

[43] M. Thiery, V. Baroghel-Bouny, N. Bourneton, G. Villain, C. Stéfani, Modélisation du séchage des bétons, Revue Européenne de Génie Civil 11 (2007) 541–577.

[44] M. van Genuchten, A closed-form equation for predicting the hydraulic conductivity of unsaturated soils, Soil Science of America Journal 44 (1980) 892–898.

[45] Y. Mualem, A new model for predicting the hydraulic conductivity of unsaturated porous media, Water resources research 12 (1976) 513–522.

[46] R. J. Millington, J. P. Quirk, Permeability of porous solids, Trans. Faraday Soc. 57 (1961) 1200–1207.

[47] S. Poyet, S. Charles, N. Honoré, V. L'hostis, Assessment of the unsaturated water transport properties of an old concrete: Determination of the pore-interaction factor, Cement and Concrete Research 41 (2011) 1015–1023.

[48] C. Zhou, Predicting water permeability and relative gas permeability of unsaturated cement-based material from hydraulic diffusivity, Cement and Concrete Research 58 (2014) 143 – 151.

[49] T. C. Powers, The thermodynamics of volume change and creep, Matériaux et Construction 1 (1968) 487–507.

[50] F. Beltzung, F. Wittmann, Role of disjoining pressure in cement based materials, Cement and Concrete Research 35 (2005) 2364–2370.

[51] B. V. Derjaguin, Some results from 50 years' research on surface forces, in: Surface Forces and Surfactant Systems, Steinkopff, Darmstadt, 1987, pp. 17–30.

[52] V. Baroghel-Bouny, M. Mainguy, T. Lassabatere, O. Coussy, Characterization and identification of equilibrium and transfer moisture properties for ordinary and high-performance cementitious materials, Cement and Concrete Research 29 (1999) 1225–1238.

[53] D. Gawin, F. Pesavento, B. A. Schrefler, Modelling creep and shrinkage of concrete by means of effective stresses, Materials and Structures 40 (2007) 579–591.

[54] O. Coussy, P. Dangla, T. Lassabatère, V. Baroghel-Bouny, The equivalent pore pressure and the swelling and shrinkage of cement-based materials, Materials and Structures 37 (2004) 15–20.

[55] C. Di Bella, M. Wyrzykowski, P. Lura, Evaluation of the ultimate drying shrinkage of cement-based mortars with poroelastic models, Materials and Structures 50 (2016) 52.

[56] H. Ye, A. Radlińska, A review and comparative study of existing shrinkage prediction models for portland and non-portland cementitious materials, Advances in Materials Science and Engineering 2016 (2016).

[57] Benboudjema, F., Torrenti, J.-M., Modelling desiccation shrinkage of large structures, EPJ Web of Conferences 56 (2013) 02001.

[58] F. Benboudjema, F. Meftah, J.-M. Torrenti, A viscoelastic approach for the assessment of the drying shrinkage behaviour of concrete, Materials and Structures 40 (2007) 163–253.

[59] J. Brooks, A. Neville, A comparison of creep, elasticity and strength of concrete in tension and in compression, Magazine of Concrete Research 29 (1977) 131–141.

[60] C. E. Ali, Iqbal et Kesler, Mechanisms of creep in concrete, ACI Special Publication 9 (1964) 35–63.

[61] P. Rossi, J.-L. Tailhan, F. L. Maou, Comparison of concrete creep in tension and in compression: Influence of concrete age at loading and drying conditions, Cement and Concrete Research 51 (2013) 78 – 84.

[62] J. Mazars, A description of micro- and macroscale damage of concrete structures, Engineering Fracture Mechanics 25 (1986) 729–737.

[63] G. Pijaudier-Cabot, J. Mazars, J. Pulikowski, Steel-concrete bond analysis with nonlocal continuous damage, Journal of Structural Engineering 117 (1991) 862–882.

[64] P. H. Feenstra, R. De Borst, A composite plasticity model for concrete, International Journal of Solids and Structures 33 (1996) 707 – 730.

[65] A. Hillerborg, M. Modéer, P.-E. Petersson, Analysis of crack formation and crack growth in concrete by means of fracture mechanics and finite elements, Cement and Concrete Research 6 (1976) 773–782.

[66] S. H. Kosmatka, B. Kerkhoff, W. C. Panarese, Design and control of concrete mixtures, volume 15^{th}, Portland Cement Assoc., Skokie, IL, 2002.

[67] I. Yurtdas, N. Burlion, J.-F. Shao, A. Li, Evolution of the mechanical behaviour of a high performance self-compacting concrete under drying, Cement and Concrete Composites 33 (2011) 380 – 388.

[68] S. Philajavaara, A review of some of the main results of a research on the aging phenomena of concrete: effect of moisture conditions on strength, shrinkage and creep of mature concrete, Cement and Concrete Research 4 (1974) 761–771.

[69] V. Kanna, R. Olson, H. Jennings, Effect of shrinkage and moisture content on the physical characteristics of blended cement mortars, Cement and Concrete Research 18 (1998) 1467–1477.

[70] M. Biot, D. Willis, The elastic coeff cients of the theory of consolidation, Journal of Applied Mechanics 15 (1957) 594–601.

[71] E. Galenne, B. Masson, A new mock-up for evaluation of the mechanical and leak-tightness behaviour of npp containment building, Proc., CCSC 2012 (2012).

[72] Électricité de France, Site web projet VeRCoRs, 2012.

[73] L. Charpin, Y. L. Pape, É. Coustabeau, É. Toppani, G. Heinfling, C. L. Bellego, B. Masson, J. Montalvo, A. Courtois, J. Sanahuja, N. Reviron, A 12 years edf study of concrete creep under uniaxial and biaxial loading, Cement and Concrete Research (2017).

[74] J. Carette, F. Soleilhet, F. Benboudjema, X. Ma, G. Nahas, K. Abahri, A. Darquennes, R. Bennacer, Identifying the mechanisms of concrete drying: An experimental-numerical approach, Construction and Building Materials 230 (2020) 117001.

[75] S. Poyet, Determination of the intrinsic permeability to water of cementitious materials: influence of the water retention curve, Cement and Concrete Composites 35 (2013) 127–135.

649 [76] Z. Wu, H. Wong, N. Buenfeld, Transport properties of concrete after drying-
650 wetting regimes to elucidate the effects of moisture content, hysteresis and
651 microcracking, Cement and Concrete Research 98 (2017) 136 – 154.

652 [77] P. Souyris, Prédiction des propriétés poro-élastiques et de sorption d'eau en
653 fonction du développement de la microstructure des matériaux cimentaires,
654 Ph.D. thesis, Université de Toulouse, Université Toulouse III-Paul Sabatier,
655 2012.

656 [78] B. Bary, G. Ranc, S. Durand, O. Carpentier, A coupled thermo-hydro-
657 mechanical-damage model for concrete subjected to moderate temperatures,
658 International journal of heat and mass transfer 51 (2008) 2847–2862.

659 [79] D. Gawin, F. Pesavento, B. A. Schrefler, Hygro-thermo-chemo-mechanical mod-
660 elling of concrete at early ages and beyond. part ii: shrinkage and creep of con-
661 crete, International Journal for Numerical Methods in Engineering 67 (2006)
662 332–363.